

Introduction

The Tharsis rise represents one of the most significant topographic features on Mars and the most significant long-wavelength geoid anomaly [1]. Two main models have been proposed to explain the long-wavelength topography associated with Tharsis. Either a buoyant mantle plume may be supporting Tharsis from below [2], or the topography is due to an incompletely compensated volcanic construction [3]. Analysis considering both surface and buoyancy loading of the lithosphere shows that dynamic topography can generate no more than 15% of the observed long-wavelength geoid for a reasonable lithospheric thickness (100 - 200 km) [4]. However, the extent to which plume buoyancy can contribute to the observed geoid and topography depends on the elastic lithospheric thickness, T_e and the depth, D_p of the long-wavelength components of plume buoyancy.

We formulated a finite-element convection model with a temperature- and depth-dependent viscosity to study the relationship between T_e and D_p , and their effects on the dynamic geoid. We found that for a large parameter space in Rayleigh number, activation energy, activation volume, and heating mode, D_p is about 1.8 times T_e .

Since the convection models assume a purely viscous rheology, we apply an elastic filter to the resulting surface topography to account for the flexural effects of the lithosphere. The reduction in surface topography and associated geoid caused by this filtering cancels the geoid from the plume buoyancy nearly perfectly. The total dynamic geoid is very small (<25 m) at degree 4 and negative (-50 m) at degree 2. The ratio of geoid to topography at these wavelengths is also quite small (<2%). We find that although internal loading can dynamically support a large fraction of the observed topography, it fails to reproduce the geoid or the ratio of geoid to topography. We conclude that the plume buoyancy cannot be a dominant mechanism for the present-day support of Tharsis.

Modeling

We used a finite-element convection code, Citcom [5] to solve the conservative equations of mass, momentum, and energy in axisymmetric spherical geometry [6]. The mantle was heated both from below and within and cooled from above. The viscosity was both temperature and depth-dependent, following an Arrhenius Law. Evolving the equations until the system reached a steady state, we were able to generate long-wavelength mantle plumes, determine the depth to which they rose and relate that depth to the lithospheric thickness.

Mantle convection models treat the entire mantle as a purely viscous medium and the dynamic topography is determined by the viscous normal stresses at the boundaries [2].

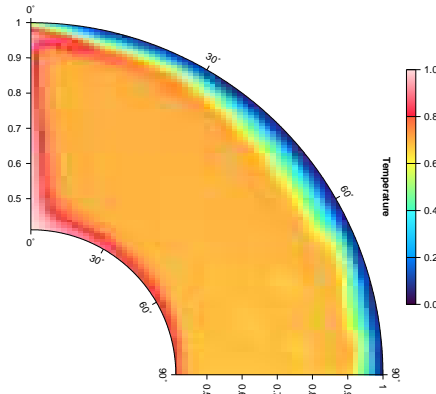


Figure 1: Long-wavelength thermal plume structure ($Ra=5 \times 10^8$, $E=150$ kJ/mol, $V=3$ cm³/mol, $Q=5 \times 10^{-9}$ W/m³).

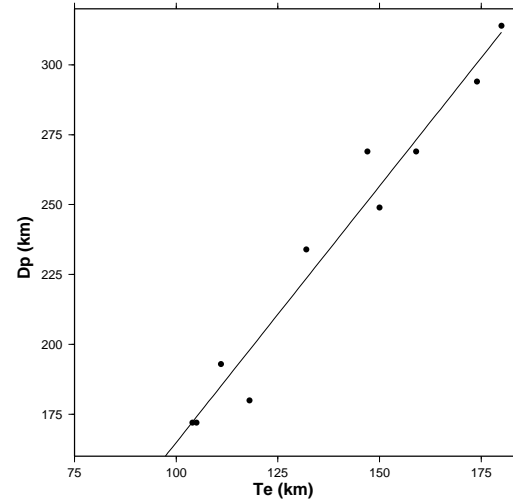


Figure 2: Plume depth vs. Elastic thickness for 10 different convection models. The solid line is a linear fit to the points with a slope of 1.83.

Although this treatment is sufficient for the core-mantle boundary (CMB) topography, it tends to overestimate the surface topography. Because the Martian lithosphere is relatively thick, a significant portion of the buoyancy forces from an upwelling plume will produce elastic stresses in the lithosphere, rather than topography. The elastic lithosphere effectively acts as a filter on the topography [7]. We include this effect by apply-

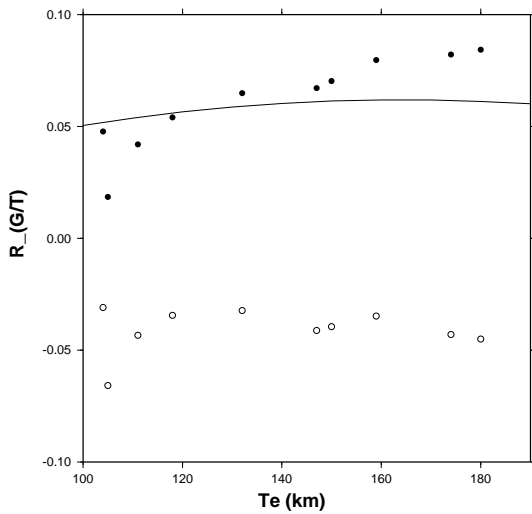


Figure 3: Dependence of dynamic topography (a), geoid (b) and $R_{G/T}$ (c) on T_e for $\ell=2$. Solid and open circles are the results before and after the elastic filtering. Solid line represents the results from an earlier loading model by Zhong and Roberts [4].

ing the viscous normal stresses determined from the convection calculations as a load to an elastic shell [4,6]. The deformation of this shell in response to that load represents the viscoelastic topography and is reduced with respect to the viscous case.

Results

Using a temperature and depth-dependent viscosity, our models produced an upwelling plume at the pole (e.g. Figure 1). A mantle plume rises along a narrow conduit from the CMB. As it approaches the stagnant lid, the buoyant material spreads out into a long-wavelength ($\ell = 2-4$) plume head. We ran ten different models with a wide variation of Rayleigh numbers, activation energy, activation volume, and heating mode. Each model resulted in a long-wavelength plume head just below the stagnant lid. For each case, we defined the depth, D_p of long-wavelength plume buoyancy to be the geometric centroid of the plume head. D_p for our models ranged between 170 km and 320 km.

The base of the stagnant lid represents the shallowest depth to which plume material may rise. Because the rheological parameters control the thickness of the stagnant lid and the elastic lithosphere, we expected to find a relationship between T_e and D_p . Defining T_e as the depth to the 500°C isotherm [8], we found that our cases had T_e between 100 and 180 km. Plotting D_p against T_e for each case, we found that the relationship between these parameters is indeed linear with a slope of 1.83 (Fig. 2). We expect that this relationship is not very sensitive to the choice of the isotherm used to define T_e .

For each case, we calculated the dynamic topography at the surface both with and without the elastic filtering. We find that in general, the surface topography increases with T_e and

that including the elastic stresses in the lithosphere reduces the topography by about 25%. We then calculated the total geoid at the surface due to the surface topography, CMB topography, and the plume material in the mantle. When the elastic lithosphere is ignored, the plume buoyancy is completely compensated by the topography. The mass deficit of the plume is roughly equal to the mass excess of the topography. Because the topography is at the surface and the plume is at depth, the topography contributes more to the geoid at the surface. The net geoid is positive. When the elastic filter is applied, the topography is reduced and so is the topographic contribution to the geoid. The plume is unaffected by the filter. We find that the geoid contributions from the plume and the topography nearly cancel each other when the elastic lithosphere is considered. In fact, at $\ell = 2$, the net geoid is slightly negative, which is inconsistent with the observations. Finally, we calculated the ratio of geoid to topography, $R_{G/T}$ for our cases. Because the geoid and topography are highly correlated on Mars [9], the observed $R_{G/T}$ is relatively high ($R_{G/T}=0.30$ at $\ell=2$) [4]. Because the geoid determined from the filtered topography is extremely low (-50 m), $R_{G/T}$ is also low (0.03) and not consistent with the observed values. Even without the elastic filtering however, $R_{G/T}$ is still more than three times smaller than the observed value. (Fig. 3)

Discussions

From ten different convection models spanning a wide range of rheological parameters and convective vigor, we found that T_e ranges between about 100 km and 180 km, consistent with values inferred from gravity and topography modeling [9]. We find that the ratio of D_p to T_e is constant and roughly equal to 1.8. We found that although the dynamic topography produced by plume buoyancy approaches the observed values, the associated geoid is insufficient to explain the observed geoid anomalies over Tharsis. When the elastic stresses in the lithosphere are included, the dynamic topography is significantly reduced. The geoid and $R_{G/T}$ are reduced almost to zero and may even be negative for degree 2.

Our results suggest that dynamic uplift by a mantle plume cannot sufficiently explain the observed geoid and topography anomalies associated with the Tharsis rise. We do not suggest that there is no plume underneath Tharsis; only that such a plume cannot create a significant geoid anomaly. Our results support the idea that the Tharsis rise results from a volcanic construction loading an elastic lithosphere [3].

References

- [1] Zuber and Smith (1997) *J. Geophys. Res.* 102, 28,673. [2] Harder and Christensen (1996) *Nature* 380, 507. [3] Phillips et al. (2001) *Science* 291, 2587. [4] Zhong and Roberts (2003) *Earth Planet. Sci. Lett.* 214, 1. [5] Moresi and Solomatov (1995) *Phys. Fluids* 7, 2154. [6] Zhong (2002) *J. Geophys. Res.* 107, 10.1029/2001JE001589. [7] Turcotte et al. (1981) *J. Geophys. Res.* 86, 3951. [8] Watts et al. (1980) *Nature* 283, 532. [9] McGovern et al. (2002) *J. Geophys. Res.* 107, 10.1029/2002JE001854.